AGU ADVANCING EARTH AND SPACE SCIENCES

Geophysical Research Letters®

RESEARCH LETTER
10.1029/2022GL097864

Helicopter-Based Ocean Observations Capture Broad Ocean Heat Intrusions Toward the Totten Ice Shelf

Yoshihiro Nakayama[1], Pat Wongpan[1,2,3], Jamin S. Greenbaum[4], Kaihe Yamazaki[1,5], Tomohide Noguchi[6], Daisuke Simizu[5], Haruhiko Kashiwase[7], Donald D. Blankenship[8], Takeshi Tamura[5,9], and Shigeru Aoki[1]

[1]Institute of Low Temperature Science, Hokkaido University, Sapporo, Japan, [2]Australian Antarctic Program Partnership, Institute for Marine and Antarctic Studies, University of Tasmania, nipaluna/Hobart, TAS, Australia, [3]JSPS International Research Fellow, Japan Society for the Promotion of Science, Tokyo, Japan, [4]Scripps Institution of Oceanography, University of California, San Diego, La Jolla, CA, USA, [5]National Institute of Polar Research, Tachikawa, Japan, [6]Marine Works Japan Limited, Yokosuka, Japan, [7]National Institute of Technology, Tomakomai College, Tomakomai, Japan, [8]Institute for Geophysics, University of Texas at Austin, Austin, TX, USA, [9]The Graduate University for Advanced Studies, Tachikawa, Japan

Abstract The recent discovery of warm ocean water near the Totten Ice Shelf (TIS) has increased attention to the Sabrina Coast in East Antarctica. We report the result of 6-day helicopter-based observations conducted during the 61st Japanese Antarctic Research Expedition (JARE61), revealing warm ocean water (0.5–1°C) occupying a large previously unsampled area of the Sabrina Coast (116.5°E–120°E) below 550–600 m. Along the TIS front, we observe modified Circumpolar Deep Water (mCDW) well above freezing (~−0.7°C), consistent with previous work. We identify glacial meltwater outflow from the TIS cavity west of 116°E. No signs of mCDW intrusions toward the Moscow University Ice Shelf cavity are observed; however, those observations were limited to only two shallow (~330 m) profiles. We also highlight the advantages of helicopter-based observations for accessibility, speed, maneuverability, and cost-efficiency. The combination of ship- and helicopter-based observations using the JARE61 approach will increase the potential of future polar oceanographic observations.

Plain Language Summary Totten Glacier hosts the most rapidly thinning ice in East Antarctica. This record of thinning is due to rapid melt along the grounding line of the Totten Ice Shelf (TIS), where warm ocean water from the open ocean flows into ice shelf cavities. To understand the pathways and mechanisms of warm water inflow, ocean observations for entire continental shelf regions are necessary. This has historically not been possible due to intense sea ice and icebergs in the region. To overcome this problem, we conducted a 6-day helicopter-based oceanographic campaign during the 61st Japanese Antarctic Research Expedition. Our measurements show that warm ocean water occupies a large area of the continental shelf off the TIS. We identify glacial meltwater outflow from the TIS cavity west of 116°E, which provides direct evidence of TIS melting. We also show that helicopter-based measurements are better for the following aspects; (a) helicopter operations are insensitive to sea ice conditions, (b) helicopter travels faster than a ship, (c) helicopter can conduct measurement in a small ice crack, and (d) helicopter is cheaper to operate than an ice breaker. By combining ship-based and helicopter-based approaches, we may be able to enhance the efficiency of future polar oceanographic observations.

Pat Wongpan and Jamin S. Greenbaum contributed equally to this work.

Key Points:

- Six-day helicopter-based observations retrieved 67 temperature profiles covering the entire continental shelf region off the Totten Ice Shelf (TIS)
- Between 116.5°E and 120°E, modified Circumpolar Deep Water can be found uniformly over the continental shelf region below 550–600 m
- Glacial meltwater outflow from the TIS cavity is identified west of 116°E

Supporting Information:

Supporting Information may be found in the online version of this article.

Correspondence to:

Y. Nakayama,
Yoshihiro.Nakayama@lowtem.hokudai.ac.jp

Citation:

Nakayama, Y., Wongpan, P., Greenbaum, J. S., Yamazaki, K., Noguchi, T., Simizu, D., et al. (2023). Helicopter-based ocean observations capture broad ocean heat intrusions toward the Totten Ice Shelf. *Geophysical Research Letters*, *50*, e2022GL097864. https://doi.org/10.1029/2022GL097864

Received 20 JAN 2022
Accepted 12 JUN 2022

1. Introduction

Intrusions of warm ocean water toward peripheral Antarctic ice shelves were discovered in the Amundsen Sea in 1994 (Jacobs et al., 1996). After ~30 years of oceanographic observations, intrusions of warm ocean water toward Antarctic ice shelves are observed in the Amundsen Sea, Bellingshausen Sea, Weddell Sea, and along the East Antarctic coast (e.g., Dutrieux et al., 2014; Jacobs et al., 2011; Nakayama et al., 2013; Rintoul et al., 2016; Ryan et al., 2020; Thompson et al., 2018, 2020). However, oceanographic observations over Antarctic continental shelves are still challenging due to harsh environments in polar regions and complex logistics. For example, oceanographic observation seasons in Antarctica are typically limited to about 3 months during the austral summertime. Even during that period, sea ice remains on the Antarctic continental shelf (Cavalieri et al., 2006), impeding ship navigation. In the vicinity of the ice shelves, many icebergs are commonly observed, in some areas making

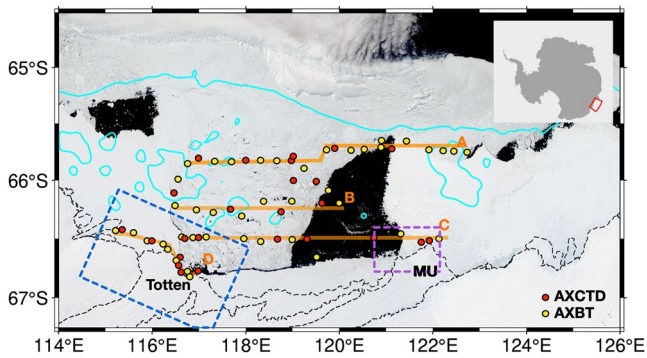

Figure 1. MODIS/Aqua image from 15 December 2019, off the Totten and Moscow University (MU) ice shelves. The red and yellow solid dots indicate the position of Airborne eXpendable Conductivity, Temperature, and Depth and Airborne Bathy-Thermograph stations, respectively, conducted during the 61st Japanese Antarctic Research Expedition (during the 2019–2020 austral summer season). The lines marked A–D are the sections discussed in this work. Ice shelf front and coastline are shown by dashed and solid lines, respectively. The 1,000-m contour is shown in cyan. The upper-right panel shows Antarctica with the enclosed region denoting the location of the enlarged portion. Close-ups for the regions enclosed by blue and purple lines are shown in Figures 4a and 4b, respectively. Ice front and grounding lines are shown by the dashed lines.

it impossible for ships to penetrate these areas (Hamley & Budd, 1986). As a result, we are still far from understanding pathways, magnitude, and mechanism of warm ocean heat intrusions toward Antarctic ice shelves.

The Totten Glacier Catchment (Figure 1) holds an ice volume equivalent of ∼3.5 m of global sea-level rise in marine-based ice (Greenbaum et al., 2015). The grounding line of the Totten Ice Shelf (TIS) is remarkably deep at the depth of about 2,000 m. The TIS grounding line has been observed to be retreating (Li et al., 2016; Rignot et al., 2019) and regional mass loss has been observed (Velicogna et al., 2014). Oceanographic observations at the ice shelf front were successfully conducted in 2015 for the first time, revealing that modified Circumpolar Deep Water (mCDW) of ∼−0.4°C can reach the TIS (Rintoul et al., 2016) through seafloor troughs entering the ice shelf cavity (Greenbaum et al., 2015). However, oceanographic and bathymetric surveys over the continental shelf along the likely mCDW pathways are completely missing due to intense sea ice cover and icebergs.

Polar oceanographic measurements using AXCTD (Airborne eXpendable Conductivity, Temperature, and Depth) and AXBT (Airborne Bathy-Thermograph) have a long history of development. For the Arctic Ocean, Childers and Brozena (2005) suggested pan-Arctic observations using long-range aircraft observations. McPhee et al. (2009) conducted an extensive hydrographic survey in the Canadian Basin of the Arctic Ocean including 7 AXCTDs. Recently, airborne oceanographic observations have been deployed for studying sea ice and near-surface ocean processes (e.g., Dewey et al., 2017; Zhang et al., 2016). Around Greenland, AXCTDs are widely used by NASA's Ocean Melting Greenland (OMG) project, which collected over ∼100 profiles each year since 2016. Recent papers utilize AXCTD observations to conclude that different oceanographic conditions are observed for different fjords (An et al., 2019, 2021; Holland et al., 2008; Khazendar et al., 2019; Rignot et al., 2021). For Antarctica, helicopter-supported oceanography has a long history (e.g., Gordon et al., 1993; Ohshima et al., 1996; Van Caspel et al., 2015) and is utilized for example, as part of the Ice Station Weddell Program. Airborne oceanographic observations using expendable instruments are starting recently, for example, East Antarctic Grounding Line Experiment (EAGLE) Project and International Collaborative Exploration of the Cryosphere by Airborne Profiling (ICECAP).

In this work, we show the results of 6-day helicopter-based oceanographic observations from the Japanese icebreaker Shirase in December 2019. We further discuss the capability and potential of helicopter-based missions for identifying ocean heat pathways toward Antarctic ice shelves. The utilization of the ship-based oceanographic observations from icebreaker Shirase (AGB5003) in the 2019–2020 austral summer season is limited to the evaluation and comparison of helicopter-based observations purposes only. Please refer to Hirano et al. (2023) for a joint analysis of helicopter- and ship-based oceanographic measurements from the 61st Japanese Antarctic Research Expedition (JARE61).

2. Data and Method

2.1. Helicopter-Based Observations

AXCTD (Tsurumi-Seiki, Kanagawa, Japan) and AXBT (Sparton, Ultra Electronics) were deployed in December 2019 from CH101 Helicopters operating from the Japanese ice breaker Shirase during JARE61. In total 28 AXCTD and 47 AXBT probes were deployed. These expendable instruments were launched from a helicopter, fell under a small parachute, and floated on the ocean surface after impact (Movie S1). The floating portion released a probe, which sunk toward the sea bed. The AXBT probes measured temperature and the AXCTD probes measured temperature and conductivity as a function of time. The accuracies of AXCTD temperature and salinity sensors are 0.02°C and 0.026, respectively. The accuracy of the AXBT temperature sensor is 0.55°C. This information was transmitted by radio to the helicopter and recorded as audio frequency data. This audio data was converted to profile data using an MK-21 converter (Lockheed Martin Sippican) after flight operations. During

the conversion, profile depth is calculated from elapsed time by a well-known drop rate, yielding ∼2% depth accuracy (10–20 m over the continental shelf) if the sound file is flawless. Both AXBT and AXCTD are capable of profiling up to 1,000 m, and thus the seafloor depth may also be inferred from each profile data following Bailey et al. (1994). We were able to retrieve the data successfully from ∼89% of deployed AXCTD and AXBT probes. This includes four AXCTD salinity profiles showing large biases (with surface salinity higher or lower than surrounding profiles by 0.5).

2.2. Other Data

Ship-based oceanographic observations for the continental shelf region have been conducted by the Australian and American cruises in 2015 and by the Japanese cruise in 2018 (Hirano et al., 2023; Nitsche et al., 2017; Rintoul et al., 2016). These datasets highlight the coverage of previous oceanographic observations. We also use CTD and XCTD data from JARE61 to evaluate AXCTD/AXBT data quality (see Section 3.1).

3. Results

3.1. Evaluation of AXCTD and AXBT Measurements

We compare helicopter-based AXBTs and ship-based XCTDs (Figure S1a in Supporting Information S1). XCTD and AXBT stations are located within ∼5 km from 120.87°E and 65.7°S (Table S1 in Supporting Information S1). For XCTD profiles, surface temperatures exceed −0.5°C and temperature steeply drops to ∼−1.9°C from the surface to ∼50 m. From 50 to 350 m, XCTD temperatures remain near freezing point at ∼−1.9°C, corresponding to Winter Water (WW). Below 350 m, temperature increases by ∼0.4°C, showing signs of mCDW intrusions near the bottom. Two AXBT profiles show similar vertical hydrographic structures with XCTD profiles. Differences can be seen close to the surface and near the bottom. Such differences are expected because (a) vertical temperature structures close to the surface are influenced strongly by varying sea ice concentration and atmospheric conditions and (b) intrusions of mCDW are likely influenced by the local bathymetry. We also compare AXCTD and AXBT probes deployed from icebreaker Shirase with ship-based CTDs, and XCTDs (Figures S1b and S1c in Supporting Information S1).

Overall, AXBT and AXCTD profiles capture hydrographic structures with near-bottom warming. As shapes of vertical profiles are sufficient to detect warm and cold water masses, these results indicate that all AXBT and AXCTD profiles are useful for detecting subsurface ocean heat pathways toward Antarctic ice shelves (Figure S1 in Supporting Information S1). We note that absolute values of temperature and salinity can be subjected to large biases (Figure S1 in Supporting Information S1). Most analyses in this manuscript are based only on the shape of vertical profiles allowing us to differentiate WW and mCDW.

3.2. On-Shelf Observations

We describe helicopter-based observations and discuss hydrographic structures on the continental shelf off the TIS. We only show in-situ temperature because salinity is lacking for most profiles.

For the east-west section along 65.7°S (Section A in Figures 1 and 2a), we find a gentle westward deepening continental slope. Cold WW occupies the top 400–600 m of the water column (Figure 2a). For the profiles west of 121.8°E, a thin layer of mCDW can be found close to the bottom. The mCDW layer thickness is ∼50 m at the shallower (eastern) part, while the mCDW layer thickness becomes ∼100 m or thicker for deeper stations. No mCDW can be found for profiles east of 121.8°E.

For the east-west vertical section located along 66.3°S (Section B), we find a steep change in profile depths at 119°E from 600–800 to 450–550 m (Figure 2b). Similar to section A, we find mCDW below 500 m depth for profiles west of 119°E but mCDW cannot be detected for shallow profiles east of 119°E.

For the east-west section located along 66.5°S (Section C), bathymetry is shallow (200–300 m) between 120°E−121.5°E (Figure 2c). For those profiles between 120°E−121.5°E, the temperature remains close to the freezing point from the surface to the bottom. We again find a steep change in bathymetry at 119.5°E, where water depth changes from 350 m to deeper than 600 m, consistent with Silvano et al. (2017); Silvano et al. (2018, 2019). Similar to sections A and B, we find mCDW below 500 m depth with a mean temperature of 0.54°C

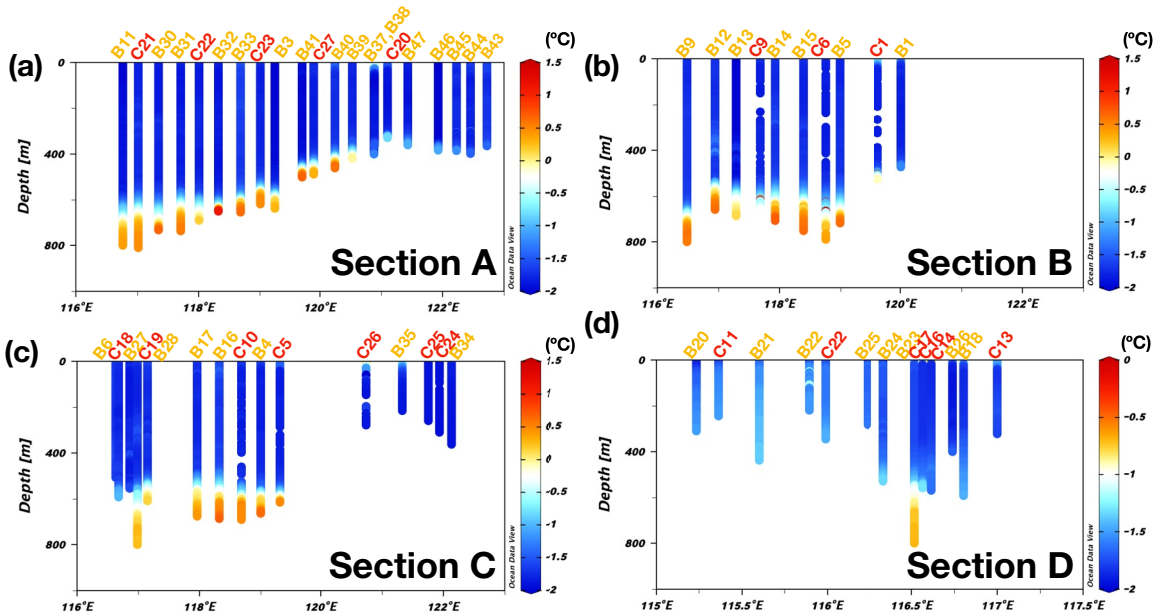

Figure 2. (a–d) are vertical temperature profiles for Sections A–D in Figure 1, respectively. Note that the plotted longitude range and color scales are different for (d). This figure is created using Ocean Data View (Schlizer, 2017).

(averaged for stations between 117.5°E–119.5°E) and the maximum temperature of 0.7°C observed at station B16 (Figure 2). We also note that bathymetry becomes slightly deeper (e.g., 350 m at stations B24 and C34) at the eastern part of section C, close to the Moscow University Ice Shelf (MUIS) front. For these profiles, water temperature remains at ∼−1.9°C from the surface to the bottom.

3.3. Ice Shelf Front Observations

3.3.1. Totten Ice Shelf Front

We deployed AXCTD and AXBT sensors along the TIS front east of 116.5°E and within a landfast sea ice (fast ice) crack west of 116.5°E (Figures 3b, 4a, and 4c). By using helicopters, we were able to deploy AXCTD and AXBT probes extremely close to the ice shelf front within 1 km (Figure 4a, e.g., stations C17, C14, and B18). We were also able to drop our probes in the narrow fast ice crack with averaged and minimum widths of ∼100 and ∼30 m, respectively (Table S2 in Supporting Information S1). No other cracks could be found in the area (Figure 4c). To our knowledge, no oceanographic observations were conducted previously west of ∼116°E due to the presence of multi-year and thick fast ice.

At station B23 mCDW (∼−0.7°C) is located below 600 m, showing that mCDW reaches the TIS cavity through deep troughs, similar to Rintoul et al. (2016); Hirano et al. (2023). Station B23 is at ∼116.5°E and our probe

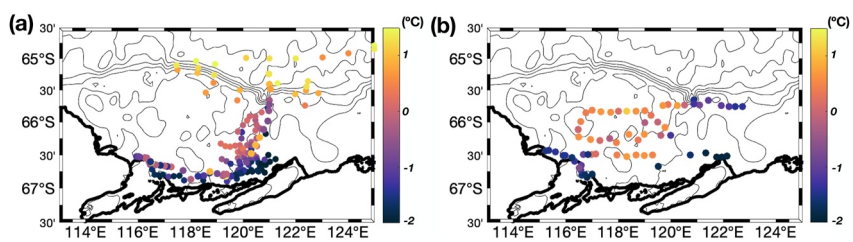

Figure 3. (a) Spatial distribution of bottom temperature based on existing observations at the time of the helicopter measurements (Nitsche et al., 2017; Rintoul et al., 2016) and 59th Japanese Antarctic Research Expedition in 2017–2018 austral summer season. (b) Spatial distribution of bottom temperature based on helicopter-based Airborne eXpendable Conductivity, Temperature, and Depth and Airborne Bathy-Thermograph observations.

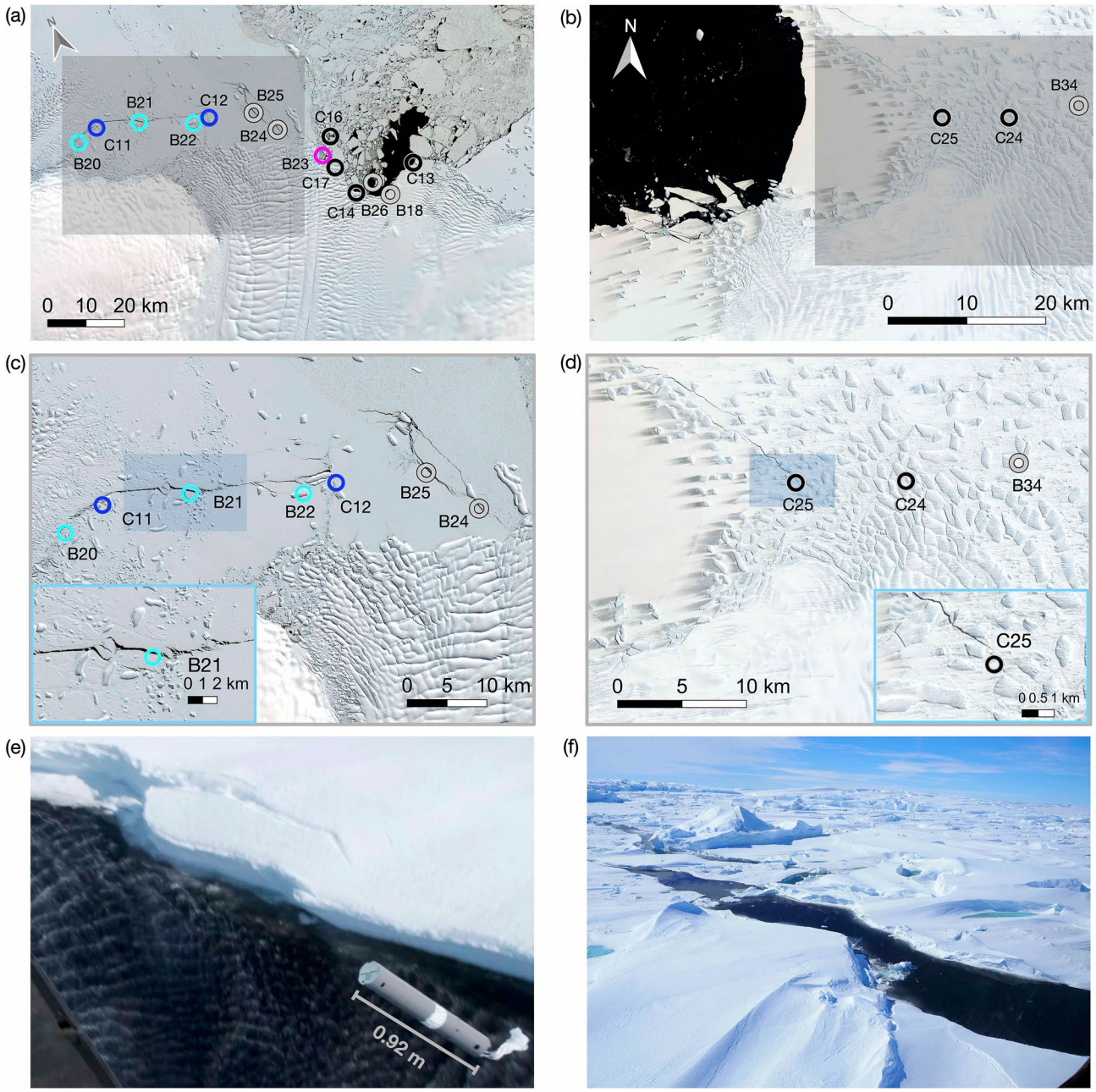

Figure 4. Deployment of Airborne Bathy-Thermograph and Airborne eXpendable Conductivity, Temperature, and Depth (AXCTD) through the sea ice cracks. (a, b) are pan-sharpening Landsat-8 images (15 m resolution) in front of Totten Ice Shelf and Moscow University Ice Shelf, respectively. (c, d) are zoom-in shots of gray-transparent patches in (a, b), respectively. The blue-framed insets in (c, d) are the second-level magnification of blue-transparent rectangles. The Landsat-8 acquisition dates of (a, c) and (b, d) are 29 and 15 December 2019, respectively. (e) Screenshot of the deployment video (see Movie S1) illustrating an AXCTD with 0.92-m long falling into an opening area of sea ice in front of Moscow University Ice Shelf. (f) A side view of the same sea ice opening from the CH101 helicopter during the operation. Figures 4a–4d was plotted using Quantarctica 3 (Matsuoka et al., 2021).

likely samples the same trough, where (Rintoul et al., 2016) observed the warmest mCDW intrusions (Figure 2 in Rintoul et al., 2016). The depth estimated from AXBT measurements (B23) is ~800 m and shallower than trough depths of ~1,100 m (Rintoul et al., 2016), likely because our measurements probe does not fall into the deepest part of the trough. We also note that the seafloor inferred from the profile depths becomes shallower to the west of 116°E (~300–400 m depths) consistent with bathymetry based on airborne gravity data (Greenbaum et al., 2015).

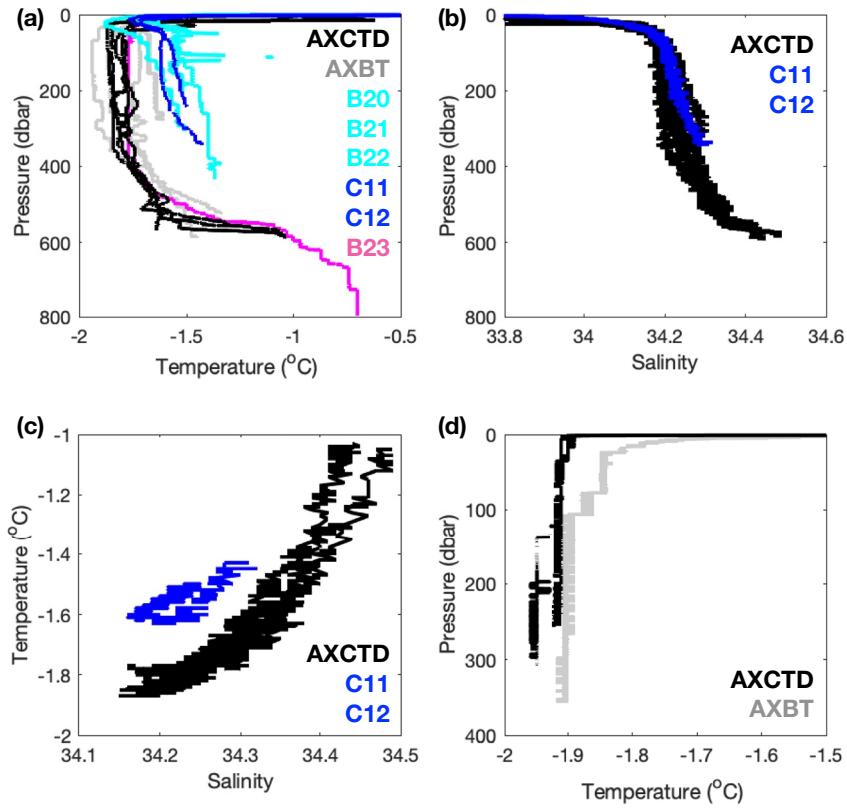

Figure 5. Vertical profiles of (a) temperature and (b) salinity for the Totten Ice Shelf (TIS) front. (c) Temperature-Salinity diagram of TIS front profiles. The top 50 m is excluded. Vertical profiles of (d) temperature for the Moscow University Ice Shelf front. In Figures 4a, 4c and 5a, 5b, and 5c Airborne eXpendable Conductivity, Temperature, and Depth and Airborne Bathy-Thermograph (AXBT) stations west of 116.1°E are shown in blue and cyan, respectively. In Figure 5a, B23 is shown in pink. Other Airborne eXpendable Conductivity, Temperature, and Depth and AXBT stations are, respectively, marked in black and gray. We note that the vertical profile of B22 shows spikes of high temperature, which may be caused by malfunctions of sensors. We are not able to remove these spikes because the accuracy of the AXBT temperature sensor is 0.55°C.

3.3.2. Moscow University Ice Shelf Front

On 19 December 2019, we attempted to conduct AXCTD and AXBT measurements near the MUIS calving front. Significant fast ice and several grounded icebergs were found near the MUIS, south of 65.8°S and east of 121.5°E. At the time we were limited to deploying AXCTD and AXBT sensors at three stations C24, C25, and B34 (Figures 4b and 4d); the sizes of ice holes were between 15 and 30 m for C24, C25, and B34 stations (Figure 4 and Table S2 in Supporting Information S1). The AXCTD and AXBT profiles near the MUIS reveal near-freezing temperatures from the surface to the bottom (Figure 5d). These are the first observations east of 121°E in front of MUIS and provide valuable information for the MUIS ocean circulation from an oceanographic perspective.

4. Discussion

4.1. Inferred Ocean Circulation From Hydrographic Structures Off the Totten and Moscow University Ice Shelves

We identify broad mCDW pathways toward the TIS. The spatial distributions of bottom temperature obtained by helicopter-based measurements show that warm mCDW (~0.5°C) are distributed over a large area of the continental shelf extending from 116.5°E to 120°E (Figure 3b). We do not find a strong temperature gradient from north to south indicating that mCDW (with temperature of ~0.5°C) broadly penetrates to ~50 km from the TIS front. The TIS front mCDW temperature was ~−0.7°C (Figure 2d), showing that intense modifications of

mCDW occur within 50 km from the TIS front or the warmest mCDW is blocked by bathymetric obstacles from getting further south. A similar conclusion was inferred from TIS front observations by Silvano et al. (2017).

We also identify glacial meltwater outflow from the TIS front west of 116°E. TIS front section also shows that western profiles tend to have higher temperatures than eastern profiles (Figure 5). Such elevated temperatures (Figure 5a) and distinctive differences in the temperature-salinity diagram (Figure 5c) similar to Nakayama et al. (2013) are typical features for glacial meltwater outflow (Biddle et al., 2019; Dutrieux et al., 2014; Jacobs et al., 2011; Nakayama et al., 2013). For example, both observations and simulations show that elevated temperature can be observed and simulated at the location of glacial meltwater outflow at the western side of the Pine Island Ice Shelf front (see Figure 5 in Nakayama et al., 2013, Figure 4 in Nakayama et al., 2021).

This analysis requires good data accuracy and biases in temperature and salinity can lead to wrong interpretation. We are still convinced that the captured meltwater signal is realistic because (a) all five profiles (three AXBTs and two AXCTDs) show consistent hydrographic signatures (Figures 5a and 5c) and (b) Silvano et al. (2017) and Hirano et al. (2023) captures outflowing glacial meltwater slightly east of 116°E likely capturing part of the glacial meltwater outflow.

For the MUIS, our measurements do not capture mCDW intrusions toward the MUIS. We do not capture glacial meltwater outflow from the MUIS either as we only observe the nearly constant temperature from the top to bottom at the MUIS front (Figure 5d). Additional observations are required to infer a conclusive picture of ocean circulation toward and away from the MUIS.

4.2. Advantages of Helicopter-Based Measurements

In contrast to previous approaches using long-range aircraft (e.g., An et al., 2019, 2021; Childers and Brozena 2005; Dewey et al., 2017; Khazendar et al., 2019; McPhee et al., 2009; Rignot et al., 2021), the helicopter approach enables deployments of AXCTD and AXBT probes into relatively small holes. For example, the average and minimum size of sea ice crack for section A west of 119.5°E are about 150 and 30 m in widths, respectively (Table S2 in Supporting Information S1). The minimum size of the hole of all observations is estimated to be 15–30 m in diameter (Table S2 in Supporting Information S1). During our flight observations, we attempted to conduct four east-west hydrographic sections (Figure 1) and we were able to complete all these sections by finding small sea ice cracks despite that most of the area was almost 100% covered by sea ice (Figure 1). At the time when helicopter-based measurements were conducted, existing observations were limited to the area close to the coast and inside the Dalton Polynya (Figure 3a); the helicopter-based measurements discussed here allow us to obtain large-scale hydrographic features of the continental shelf region, despite intense sea ice and iceberg conditions at the time (Figure 1).

Other advantages of helicopter-based measurements are speed and distance capability. Taking advantage of the flight range of the helicopter and the moving platform of the icebreaker Shirase, we could conduct oceanographic surveys of the entire continental shelf region north of the TIS, TIS front, and MUIS front. We covered ∼100 km by ∼300 km area within 6 days (in total ∼32 hr) of helicopter operations. Previously, Australian, American, and Japanese icebreakers have conducted weeks of oceanographic observations in the area (Hirano et al., 2023; Nitsche et al., 2017; Rintoul et al., 2016), but their oceanographic observations coverage is much limited when compared to that of our helicopter-based observations (e.g., Figure 3).

As helicopters are commonly on board for operational and observational purposes in most ice breakers, we suggest that quick and broad surveys using helicopters can be a good supplement for selecting targeted areas and implementing strategies for intense oceanographic observations. Typically, expenses required for helicopter-based observations are small compared to ice breaker operational costs. For JARE, a chartered helicopter for entire Antarctic operations normally costs 400,000 USD including a pilot, a technician, fuel, and 100-hr flight time. A yearly operation of the Japanese icebreakers costs ∼40 million USD. Helicopters hence provide efficient and effective measurements in addition to the ship-based detailed and higher-quality surveys including water sampling.

5. Conclusions

We report the result of 6-day helicopter-based observations revealing hydrographic features of the entire continental shelf region off the TIS. Between 116.5°E and 120°E, relatively warm mCDW can be found uniformly over the continental shelf below 550–600 m (Figure 2). At the ice shelf front, we observe mCDW of ∼−0.7°C in the deep trough, where Rintoul et al. (2016) observed warm mCDW. Glacial meltwater outflow from the TIS cavity is identified west of 116°E (Figures 5a and 5c). Our observations did not detect mCDW intrusions toward Moscow University Ice Shelf cavity; however, it may be present in troughs deeper than what we could sample and we were not able to capture glacial meltwater outflow (Figure 5d). The helicopter-based survey offers advantages in (a) access to remote or inaccessible regions for icebreakers, (b) increased speed and distance capability, and (c) capability to deploy probes in small ice cracks (less than ∼30 m). Our results emphasize the capability and effectiveness of helicopter-based oceanographic observations for efficient and broad surveys of Antarctic coastal regions, especially for tracing pathways of ocean heat intrusions toward Antarctic ice shelves.

Data Availability Statement

In-situ airborne observation data used in this study is available at https://doi.org/10.17592/001.2022061601 (Nakayama et al., 2022).

Acknowledgments

We thank the officers, crew, and scientists on board the Icebreaker Shirase. Helicopter flight operations and sensor deployments were conducted by Akihiro Naniwa, Yoshiyuki Inoue, Ken Fujitaka, Yoshiji Nitta, Shinji Sezaki, Takuya Fukumoto, Daisuke Soejima, Hiroshi Yamashita, Tetsufumi Nozawa, Keisuke Hamada, Yoshihiko Nakamura, Nobuhisa Takemoto, and Jun Mashiba. Insightful comments from the two anonymous reviewers were very helpful for improvement of the manuscript. This work is supported by the Science Program of Japanese Antarctic Research Expedition (JARE) as Prioritized Research Project (AJ0902: ROBOTICA) and National Institute of Polar Research (NIPR) through Project Research KP-303. Technical support for AXCTD/AXBT measurements was provided by Gregory Ng, Dillon Buhl, and Daniel Duncan from the University of Texas Institute of Geophysics, and by Tsurumi-Seiki Co., Ltd in Japan. We also thank Jason Roberts for their useful comments and suggestions. This work was supported by Grants-in-Aids for Scientific Research (JP17H06316, JP17H06317, JP17H06322, JP17H04710, JP21H04931, JP21K13989) from the Ministry of Education, Culture, Sports, Science, and Technology in Japan. Y.N. was also supported by the Inoue Science Research Award from the Inoue Science Foundation. J.S.G acknowledges support from NSF OPP-2114454. P.W. acknowledges support from the Australian Government as part of the Antarctic Science Collaborative Initiative program and contributes to Project 6 (Sea Ice) of the Australian Antarctic Program Partnership (project ID ASCI000002) and the Japan Society for the Promotion of Science (18F18794). J.S.G. acknowledges support from NSF grant OPP-2114454, NASA's Cryosphere Program under Grant 80NSSC22K0387, and Seequent Limited. J.G.G. and D.D.B. acknowledge support from NSF grant PLR-1543452, the G. Unger Vetlesen Foundation, Australian Antarctic Division projects 4346 and 4511, and the Australian Research Council's Special Research Initiative for Antarctic Gateway Partnership (project ID SR140300001).

References

An, L., Rignot, E., Chauche, N., Holland, D. M., Holland, D., Jakobsson, M., et al. (2019). Bathymetry of Southeast Greenland from oceans melting Greenland (OMG) data. *Geophysical Research Letters*, *46*(20), 11197–11205. https://doi.org/10.1029/2019gl083953

An, L., Rignot, E., Wood, M., Willis, J. K., Mouginot, J., & Khan, S. A. (2021). Ocean Melting of the Zachariae Isstrøm and Nioghalvfjerdsfjorden glaciers, northeast Greenland. *Proceedings of the National Academy of Sciences*, *118*(2), e2015483118. https://doi.org/10.1073/pnas.2015483118

Bailey, R., Gronell, A., Phillips, H., Tanner, E., & Meyers, G. (1994). *Quality control cookbook for XBT data, version 1.1* (p. 221). CSIRO Marine Laboratories Reports.

Biddle, L. C., Loose, B., & Heywood, K. J. (2019). Upper ocean distribution of glacial meltwater in the Amundsen Sea, Antarctica. *Journal of Geophysical Research: Oceans*, *124*(10), 6854–6870. https://doi.org/10.1029/2019jc015133

Cavalieri, D., Parkinson, C., Gloersen, P., & Zwally, H. (2006). Sea ice concentrations from Nimbus-7 SMMR and DMSP SSM/I passive microwave data.

Childers, V. A., & Brozena, J. M. (2005). Long-range aircraft as an Arctic oceanographic platform. *Deep Sea Research Part I: Oceanographic Research Papers*, *52*(12), 2366–2375. https://doi.org/10.1016/j.dsr.2005.07.004

Dewey, S. R., Morison, J. H., & Zhang, J. (2017). An edge-referenced surface fresh layer in the Beaufort Sea seasonal ice zone. *Journal of Physical Oceanography*, *47*(5), 1125–1144. https://doi.org/10.1175/jpo-d-16-0158.1

Dutrieux, P., De Rydt, J., Jenkins, A., Holland, P. R., Ha, H. K., Lee, S. H., et al. (2014). Strong sensitivity of Pine Island ice-shelf melting to climatic variability. *Science*, *343*(6167), 174–178. https://doi.org/10.1126/science.1244341

Gordon, A. L., Huber, B. A., Hellmer, H. H., & Ffield, A. (1993). Deep and bottom water of the weddell sea's western rim. *Science*, *262*(5130), 95–97. https://doi.org/10.1126/science.262.5130.95

Greenbaum, J. S., Blankenship, D., Young, D., Richter, T., Roberts, J., Aitken, A., et al. (2015). Ocean access to a cavity beneath Totten Glacier in East Antarctica. *Nature Geoscience*, *8*(4), 294–298. https://doi.org/10.1038/ngeo2388

Hamley, T., & Budd, W. (1986). Antarctic iceberg distribution and dissolution. *Journal of Glaciology*, *32*(111), 242–251. https://doi.org/10.3189/s0022143000015574

Hirano, D., Tamura, T., Kusahara, K., Fujii, M., Yamazaki, K., Nakayama, Y., et al. (2023). On-shelf circulation of warm water toward the Totten Ice Shelf in East Antarctica. *Nature Communications*, *14*. https://doi.org/10.1038/s41467-023-39764-z

Holland, D. M., Thomas, R. H., De Young, B., Ribergaard, M. H., & Lyberth, B. (2008). Acceleration of Jakobshavn Isbræ triggered by warm subsurface ocean waters. *Nature Geoscience*, *1*(10), 659–664. https://doi.org/10.1038/ngeo316

Jacobs, S. S., Hellmer, H. H., & Jenkins, A. (1996). Antarctic ice sheet melting in the Southeast Pacific. *Geophysical Research Letters*, *23*(9), 957–960. https://doi.org/10.1029/96gl00723

Jacobs, S. S., Jenkins, A., Giulivi, C. F., & Dutrieux, P. (2011). Stronger ocean circulation and increased melting under Pine Island Glacier ice shelf. *Nature Geoscience*, *4*(8), 519–523. https://doi.org/10.1038/ngeo1188

Khazendar, A., Fenty, I. G., Carroll, D., Gardner, A., Lee, C. M., Fukumori, I., et al. (2019). Interruption of two decades of Jakobshavn Isbrae acceleration and thinning as regional ocean cools. *Nature Geoscience*, *12*(4), 277–283. https://doi.org/10.1038/s41561-019-0329-3

Li, X., Rignot, E., Mouginot, J., & Scheuchl, B. (2016). Ice flow dynamics and mass loss of Totten Glacier, East Antarctica, from 1989 to 2015. *Geophysical Research Letters*, *43*(12), 6366–6373. https://doi.org/10.1002/2016gl069173

Matsuoka, K., Skoglund, A., Roth, G., de Pomereu, J., Griffiths, H., Headland, R., et al. (2021). Quantarctica, an integrated mapping environment for Antarctica, the Southern Ocean, and sub-Antarctic islands. *Environmental Modelling & Software*, *140*, 105015. https://doi.org/10.1016/j.envsoft.2021.105015

McPhee, M., Proshutinsky, A., Morison, J., Steele, M., & Alkire, M. (2009). Rapid change in freshwater content of the Arctic Ocean. *Geophysical Research Letters*, *36*(10), L10602. https://doi.org/10.1029/2009gl037525

Nakayama, Y., Cai, C., & Seroussi, H. (2021). Impact of subglacial freshwater discharge on Pine Island Ice Shelf. *Geophysical Research Letters*, *48*(18), e2021GL093923. https://doi.org/10.1029/2021gl093923

Nakayama, Y., Schröder, M., & Hellmer, H. H. (2013). From circumpolar deep water to the glacial meltwater plume on the eastern Amundsen Shelf. *Deep-Sea Research I*, *77*, 50–62. https://doi.org/10.1016/j.dsr.2013.04.001

Nakayama, Y., Yamazaki, K., Wongpan, P., Greenbaum, J. S., Noguchi, T., Tamura, T., & Aoki, S. (2022). Dataset for helicopter-based ocean observations capture broad ocean heat intrusions towards the Totten ice shelf. *Arctic Data archive System (ADS), Japan*. https://doi.org/10.17592/001.2022061601

Nitsche, F., Porter, D., Williams, G., Cougnon, E., Fraser, A., Correia, R., & Guerrero, R. (2017). Bathymetric control of warm ocean water access along the East Antarctic Margin. *Geophysical Research Letters*, *44*(17), 8936–8944. https://doi.org/10.1002/2017gl074433

Ohshima, K. I., Takizawa, T., Ushio, S., & Kawamura, T. (1996). Seasonal variations of the Antarctic coastal ocean in the vicinity of Lützow-Holm Bay. *Journal of Geophysical Research*, *101*(C9), 20617–20628. https://doi.org/10.1029/96jc01752

Rignot, E., An, L., Chauche, N., Morlighem, M., Jeong, S., Wood, M., et al. (2021). Retreat of Humboldt Gletscher, north Greenland, driven by undercutting from a warmer ocean. *Geophysical Research Letters*, *48*(6), e2020GL091342. https://doi.org/10.1029/2020gl091342

Rignot, E., Mouginot, J., Scheuchl, B., van den Broeke, M., van Wessem, M. J., & Morlighem, M. (2019). Four decades of Antarctic Ice Sheet mass balance from 1979–2017. *Proceedings of the National Academy of Sciences*, *116*(4), 1095–1103. https://doi.org/10.1073/pnas.1812883116

Rintoul, S. R., Silvano, A., Pena-Molino, B., van Wijk, E., Rosenberg, M., Greenbaum, J. S., & Blankenship, D. D. (2016). Ocean heat drives rapid basal melt of the Totten Ice Shelf. *Science Advances*, *2*(12), e1601610. https://doi.org/10.1126/sciadv.1601610

Ryan, S., Hellmer, H. H., Janout, M., Darelius, E., Vignes, L., & Schröder, M. (2020). Exceptionally warm and prolonged flow of warm deep water toward the Filchner-Ronne Ice Shelf in 2017. *Geophysical Research Letters*, *47*(13), e2020GL088119. https://doi.org/10.1029/2020gl088119

Schlitzer, R. (2017). Ocean Data View. odv.awi.de

Silvano, A., Rintoul, S. R., Kusahara, K., Peña-Molino, B., van Wijk, E., Gwyther, D. E., & Williams, G. D. (2019). Seasonality of warm water intrusions onto the continental shelf near the Totten Glacier. *Journal of Geophysical Research: Oceans*, *124*(6), 4272–4289. https://doi.org/10.1029/2018jc014634

Silvano, A., Rintoul, S. R., Peña-Molino, B., Hobbs, W. R., van Wijk, E., Aoki, S., et al. (2018). Freshening by glacial meltwater enhances melting of ice shelves and reduces formation of Antarctic Bottom Water. *Science Advances*, *4*(4), eaap9467. https://doi.org/10.1126/sciadv.aap9467

Silvano, A., Rintoul, S. R., Peña-Molino, B., & Williams, G. D. (2017). Distribution of water masses and meltwater on the continental shelf near the Totten and Moscow University ice shelves. *Journal of Geophysical Research: Oceans*, *122*(3), 2050–2068. https://doi.org/10.1002/2016jc012115

Thompson, A. F., Speer, K. G., & Schulze Chretien, L. M. (2020). Genesis of the Antarctic slope current in West Antarctica. *Geophysical Research Letters*, *47*(16), e2020GL087802. https://doi.org/10.1029/2020gl087802

Thompson, A. F., Stewart, A. L., Spence, P., & Heywood, K. J. (2018). The Antarctic Slope Current in a changing climate. *Reviews of Geophysics*, *56*(4), 741–770. https://doi.org/10.1029/2018rg000624

Van Caspel, M., Schröder, M., Huhn, O., & Hellmer, H. (2015). Precursors of Antarctic Bottom Water formed on the continental shelf off Larsen Ice Shelf. *Deep Sea Research Part I: Oceanographic Research Papers*, *99*, 1–9. https://doi.org/10.1016/j.dsr.2015.01.004

Velicogna, I., Sutterley, T., & Van Den Broeke, M. (2014). Regional acceleration in ice mass loss from Greenland and Antarctica using GRACE time-variable gravity data. *Geophysical Research Letters*, *41*(22), 8130–8137. https://doi.org/10.1002/2014gl061052

Zhang, X., Thompson, A. F., Flexas, M. M., Roquet, F., & Bornemann, H. (2016). Circulation and meltwater distribution in the Bellingshausen Sea: From shelf break to coast. *Geophysical Research Letters*, *43*(12), 6402–6409. https://doi.org/10.1002/2016gl068998